ELSEVIER

Analytical model for predicting axial capacity and behavior of concrete encased steel composite stub columns

Cheng-Chih Chen[*], Nan-Jiao Lin

Department of Civil Engineering, National Chiao Tung University, Hsinchu 30010, Taiwan

Abstract

The axial compressive capacity and force–deformation behavior of concrete encased steel stub columns were analytically investigated. An analytical model was developed for predicting the force–deformation response for composite stub columns with various structural steel sections and volumetric lateral reinforcement. Constitutive relationships were established for materials used in the composite cross section, which included unconfined concrete, partially and highly confined concrete, structural steel section, and longitudinal reinforcing bar. The axial capacity of composite stub columns can be determined from strengths contributed from each material component following the stress–strain relationship. Analytical results show that the axial load-carrying capacity and force–deformation behavior measured in the experiments can be accurately predicted. In addition to the lateral reinforcement, the structural steel section can provide a confinement effect on the concrete and enhance the axial capacity and post-peak strength.
© 2005 Elsevier Ltd. All rights reserved.

Keywords: Concrete encased; Composite column; Confined concrete

1. Introduction

Concrete encased steel columns are one type of composite columns used in composite structures. The concrete encased steel composite column consists of structural steel section encased in reinforced concrete. The structural steel is rolled or built-up shape. Deriving benefits from combining the structural steel and reinforced concrete, the composite columns possess great load-carrying capacity and stiffness owing to composite action. Further, the concrete encasement can serve for fire protection. Therefore, the use of the composite columns in medium-rise or high-rise buildings has been increased significantly in recent decades [1,2].

Numerous experimental investigations have been carried out to study the ultimate strength of concrete encased steel composite columns [3–8]. Research has also been carried out on cyclic behavior of composite beam–columns [9,10]. Although the behavior of concrete encased steel composite columns has been extensively studied, many of the research works emphasized the composite columns with H-shaped structural steel section. However, other shapes of steel section such as cross- or T-shaped are generally used in composite buildings. The composite column with cross-shaped steel section is widely used in an interior column to connect four steel beams in orthogonal directions. The cross-shaped steel section is usually fabricated by welding two H-shaped steel sections together. The composite column with T-shaped steel section is usually designed for an outer column. There is very little research regarding the effect of various shapes of steel section on the axial compressive behavior of concrete encased steel columns. The concrete confinement of composite columns with various shapes of steel section is not well understood yet.

Research has been conducted to study the confinement effect of the concrete in concrete-filled steel tube (CFT) composite columns [11–16]. From previous work, it is clear that the steel tube, particularly the circular tube, can provide confinement on concrete and lead to the enhancement of strength and ductility of the CFT columns. It is of important to investigate the concrete confinement effect in the concrete encased steel composite columns. In this study, an analytical approach is developed for determining the axial compressive load–deformation relationship for concrete encased composite stub columns. The emphasis of the proposed modeling is the

* Corresponding author. Tel.: +886 3 571 2121x54915; fax: +886 3 572 7109.
  E-mail address: chrischen@mail.nctu.edu.tw (C.-C. Chen).

Nomenclature

A_{ch}	area of the highly confined concrete;
A_{cp}	area of the partially confined concrete;
A_{cu}	area of the unconfined concrete;
A_r	cross-sectional area of the longitudinal bars;
A_s	cross-sectional area of the structural steel section;
E_c	tangent modulus of elasticity of concrete;
E_{sec}	secant modulus of the confined concrete at peak stress;
f_c	longitudinal concrete stress;
f'_{cc}	compressive strength of the confined concrete;
f_{ch}	stress of the highly confined concrete;
f'_{co}	compressive strength of the unconfined concrete;
f_{cp}	stress of the partially confined concrete;
f_{cu}	stress of the unconfined concrete;
f'_l	effective lateral confining stress;
f_s	stress of the structural steel;
f_{sr}	stress of the longitudinal bar;
f_{ys}	yield strength of the structural steel;
f_{yr}	yield strength of the longitudinal bar;
K_h	confinement factor for highly confined concrete;
K_p	confinement factor for partially confined concrete;
P_{Analy}	analytical load;
P_{Squash}	squash load;
P_{Test}	experimental load;
ε	axial compressive strain;
ε_c	longitudinal concrete strain;
ε_{cc}	strain at maximum confined concrete stress;
$\varepsilon_{cc,p}$	strain at maximum partially confined concrete stress;
ε_{co}	strain at maximum unconfined concrete stress.

establishment of stress–strain relations for concrete confined by the lateral reinforcement and various structural steel sections. The predicted axial compressive capacity and axial load–deformation relationship were compared with available experimental results to validate the analytical modeling and investigate the effect of design variables.

2. Analytical modeling

The cross section of the concrete encased steel composite column comprises three materials, i.e., concrete, structural steel, and longitudinal reinforcing bar. For a stub column, the axial compressive capacity and axial load–deformation response can be determined based on the strain compatibility on the composite cross section. When a uniform axial compressive strain is assumed, the stress of each material of the composite column can be obtained through the constitutive model established for each material. Consequently, the axial load can be calculated by adding the axial force from each material, while the axial force is computed by multiplying the stress of material by the corresponding cross-sectional area. Furthermore, the axial load versus strain curve can be
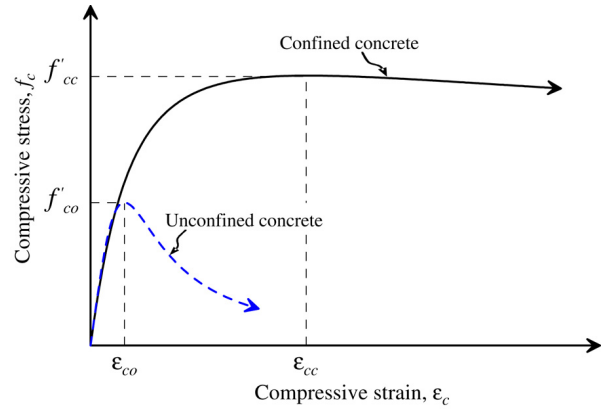

Fig. 1. Stress–strain curves for unconfined and confined concrete proposed by Mander et al. [18].

generated for the composite cross section. Several assumptions considered in this analytical model are as follows: (1) uniform distribution of compressive strain is assumed on the cross section; (2) stresses of the materials are calculated based on corresponding uniaxial stress–strain relations; (3) a confinement effect caused by the lateral reinforcement and elements of the structural steel on the concrete is considered; and (4) local buckling of the longitudinal bars and elements of the structural steel is assumed.

2.1. Constitutive model for concrete

The confinement effect of concrete by lateral reinforcement in a reinforced concrete column has been recognized because the lateral reinforcement can provide confining pressure to the concrete core [17,18]. The confining pressure results in an enhancement in the strength and ductility of the concrete, depending on the degree of the confining pressure. In addition to the lateral reinforcement, the confinement is also affected by other factors, such as distribution of the longitudinal reinforcement, cross section configuration, and loading type. Analytical models to predict the uniaxial stress–strain behavior for confined concrete have been proposed by researchers [17–19].

Mander et al. [18] proposed a unified stress–strain model, shown in Fig. 1, for confined concrete for members with different cross sections under various loading conditions. The longitudinal compressive stress–strain (f_c–ε_c) curve for confined concrete is given by

$$f_c = \frac{f'_{cc} x r}{r - 1 + x^r} \tag{1}$$

with

$$x = \frac{\varepsilon_c}{\varepsilon_{cc}} \tag{2}$$

$$r = \frac{E_c}{E_c - E_{sec}} \tag{3}$$

where f'_{cc} is the compressive strength (peak stress) of confined concrete; ε_{cc} is the strain at maximum confined concrete stress; E_c is the tangent modulus of elasticity of the concrete; and E_{sec}
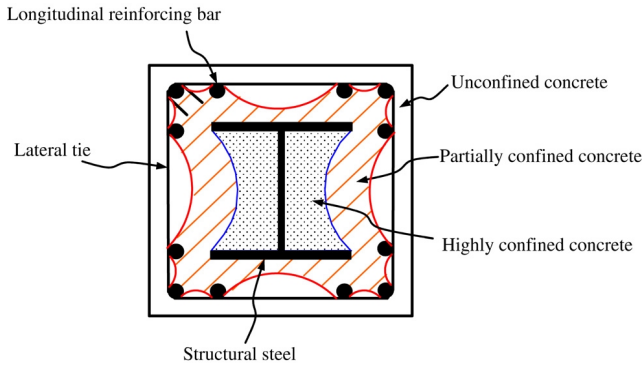
Fig. 2. Materials in a concrete encased steel composite column.

is the secant modulus of confined concrete at peak stress and is expressed as

$$E_{\text{sec}} = \frac{f'_{cc}}{\varepsilon_{cc}}. \tag{4}$$

The strain at maximum confined concrete stress ε_{cc} is suggested as

$$\varepsilon_{cc} = \varepsilon_{co} \left[1 + 5 \left(\frac{f'_{cc}}{f'_{co}} - 1 \right) \right] \tag{5}$$

where f'_{co} is the compressive strength of unconfined concrete and ε_{co} is the strain at maximum unconfined concrete stress.

Proposed by Mander et al., the compressive strength of confined concrete f'_{cc} is determined by the compressive strength of unconfined concrete f'_{co} and the effective lateral confining stress f'_l. The confined concrete strength f'_{cc} is given by

$$f'_{cc} = f'_{co} \left(-1.254 + 2.254 \sqrt{1 + \frac{7.94 f'_l}{f'_{co}}} - 2 \frac{f'_l}{f'_{co}} \right). \tag{6}$$

The effective lateral confining stress f'_l is dependent on the volumetric ratio of lateral reinforcement, configuration of the lateral and longitudinal reinforcement, and area of effectively confined concrete core. Full equations can be found in Mander et al. [18].

To determine the area of effectively confined concrete core, parabolic arching was assumed to occur between the reinforcing bars in the cross section [17,18]. Accordingly, a similar parabolic arching is assumed herein for the concrete further confined by the structural steel section. Therefore, as presented in Fig. 2, the concrete in a concrete encased steel composite section can be divided into three regions: (1) an unconfined concrete region outside the parabolic arching formed by the longitudinal bars; (2) a highly confined region inside the perimeter of the structural steel section and the arching formed by the steel section; and (3) a partially confined region inside the unconfined concrete region and outside the highly confined concrete region. Mirza and Skrabek [6], and El-Tawil and Deierlein [7] adopted a similar but simple subdivision by simplifying the arching formed for the partially confined concrete region.

Based on these three distinct regions, different stress–strain relations are assumed for the concrete. The stress–strain curve
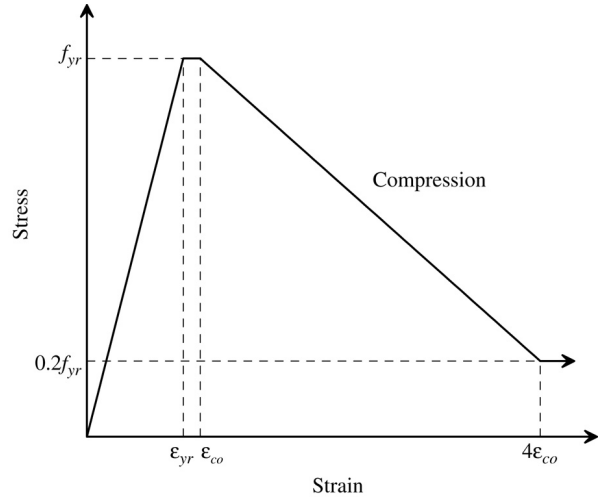

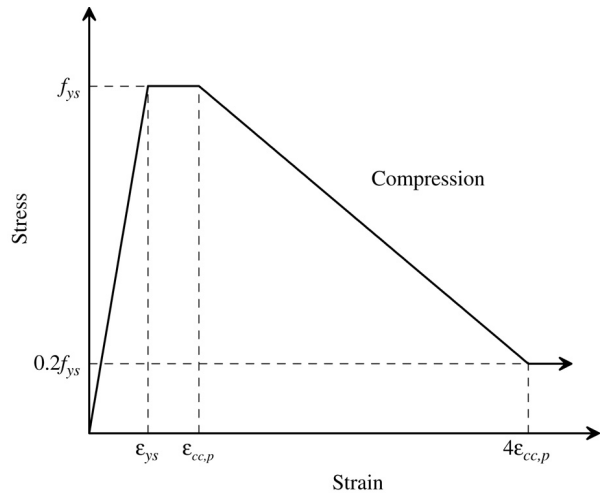Fig. 3. Stress–strain relation for longitudinal reinforcing bar in compression.

Fig. 4. Stress–strain relation for structural steel section in compression.

for unconfined concrete is determined by Eq. (1), substituting $f'_l = 0$ in Eq. (6) and $\varepsilon_{co} = 0.002$ in Eq. (5). The strength f'_{co} is taken as the concrete compressive strength measured from the cylinder test. The strain ε_{co} of 0.002 is generally acceptable for unconfined concrete [17,18]. Considering the confining stress contributed from the lateral reinforcement, the stress–strain curve for partially confined concrete can be determined as proposed by Mander et al.

In addition to the lateral reinforcement, the confining stress in the highly confined concrete region is enhanced by the structural steel section. Li et al. [9] analyzed the flexural strength of concrete encased steel composite beam–columns without considering the highly confined concrete region. However, Li et al. found that one of the reasons to underestimate the ultimate strength was that the confining effect of structural steel section on concrete was not accounted for in their analysis. Therefore, the structural steel section is taken into account in this study to determine the confining stress, and a higher compressive strength f'_{cc} is obtained for the highly confined concrete region. By considering the effect of unstiffened elements of the steel section on the confinement,
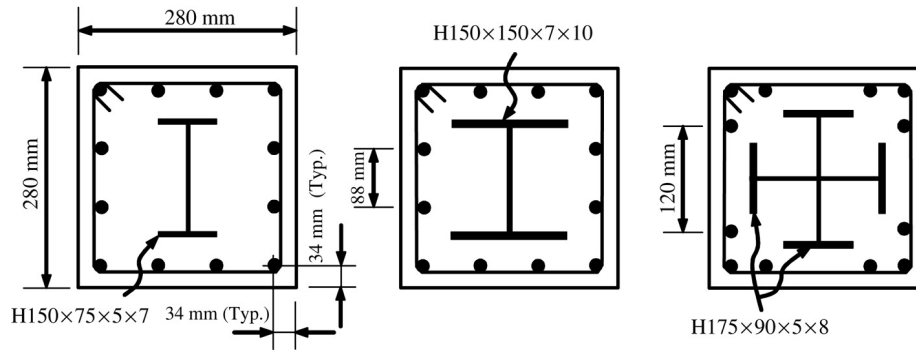
Fig. 5. Cross sections of concrete encased steel composite columns with I-, H- and cross-shaped steel sections [21,22].
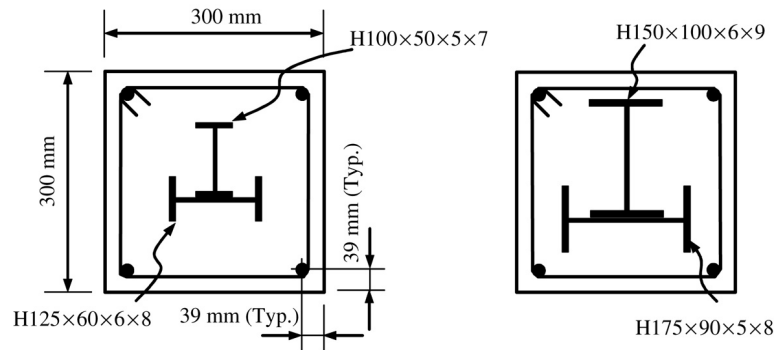

Fig. 6. Cross sections of concrete encased steel composite columns with T-shaped steel sections [23].

one-half of the corresponding steel area is taken to calculate the confining stress. In order to discuss the confinement effect, the concrete strength f'_{cc} for partially and highly confined concrete is defined as $K_p f'_{co}$ and $K_h f'_{co}$, respectively, as follows:
for partially confined concrete

$$f'_{cc} = K_p f'_{co} \tag{7}$$

for highly confined concrete

$$f'_{cc} = K_h f'_{co} \tag{8}$$

where K_p and K_h are defined as confinement factors for partially and highly confined concrete, respectively.

2.2. Constitutive model for longitudinal bar

In general, identical behavior under tension and compression is assumed for modeling the longitudinal bars in the reinforced concrete or composite members subjected to flexural bending moment [6,7]. However, buckling of the longitudinal bars occurred at large inelastic deformation when those members were subjected to axial compressive force. The buckling of the longitudinal bars greatly influences the strength and ductility of the member. As a result, load-carrying capacity and ductility of the bars decrease when the bars buckle, as observed in the tests of reinforcing bars by Bayrak and Sheikh [20].

A simple constitutive model considering the inelastic buckling of the longitudinal bars under compression is suggested herein, as presented in Fig. 3. The following assumptions are used to generate the model. The longitudinal bar under compression will reach the yield strength with a yield plateau. The stress of the bar begins to degrade when the axial strain of the bar reaches the strain ε_{co}, corresponding to the peak compressive stress f'_{co} of the unconfined concrete. It is assumed that the bar will buckle and lose its strength caused by the spalling of the concrete cover when the concrete cover reaches the peak strength. The stress of the bar will drop to 20% of its yield strength and maintain constant afterwards.

2.3. Constitutive model for structural steel section

A similar stress–strain relation as that adopted for the longitudinal bar is assumed for the structural steel section, as shown in Fig. 4. The local buckling of the elements, particularly the flanges, of the structural steel section is likely to occur after the crushing of the partially confined concrete. Therefore, stress degradation is assumed after the axial strain reaches the strain, $\varepsilon_{cc,p}$, representing the crushing of the partially confined concrete. Post-peak strength of 20% of the yield strength is assumed when the axial strain reaches four times of the strain of $\varepsilon_{cc,p}$.

3. Analytical results and discussion

3.1. Composite stub column tests

The analytical predictions of axial compressive behavior and capacity of composite stub columns are compared to experimental results. Three series of tests, matching the purpose of this study, are considered: the tests conducted by Chen and Yeh [21], by Tsai et al. [22], and by Chen et al. [23].

Table 1
Geometrical and material properties of composite stub columns

Author	Specimen	Cross section (mm)	Length (mm)	Structural steel		Longitudinal bar	Lateral tie spacing (mm)	Concrete strength f'_c (MPa)
				Shape	Size			
	SRC1	280×280	1200	H	$H150 \times 150 \times 7 \times 10$	12 No. 5	140	29.5
	SRC2	280×280	1200	H	$H150 \times 150 \times 7 \times 10$	12 No. 5	75	28.1
	SRC3	280×280	1200	H	$H150 \times 150 \times 7 \times 10$	12 No. 5	35	29.8
	SRC4	280×280	1200	Cross	Two $H175 \times 90 \times 5 \times 8$	12 No. 5	140	29.8
Chen and	SRC5	280×280	1200	Cross	Two $H175 \times 90 \times 5 \times 8$	12 No. 5	75	29.8
Yeh [21]	SRC6	280×280	1200	Cross	Two $H175 \times 90 \times 5 \times 8$	12 No. 5	35	29.5
	SRC7	280×280	1200	I	$H150 \times 75 \times 5 \times 7$	12 No. 5	140	28.1
	SRC8	280×280	1200	I	$H150 \times 75 \times 5 \times 7$	12 No. 5	75	26.4
	SRC9	280×280	1200	I	$H150 \times 75 \times 5 \times 7$	12 No. 5	140	28.1
	SRC10	280×280	1200	I	$H150 \times 75 \times 5 \times 7$	12 No. 5	75	29.8
	src1	280×280	1200	Cross	Two $H175 \times 90 \times 5 \times 8$	4 No. 5	140	23.9
	src2	280×280	1200	Cross	Two $H175 \times 90 \times 5 \times 8$	4 No. 5	100	23.5
	src3	280×280	1200	Cross	Two $H175 \times 90 \times 5 \times 8$	12 No. 5	100	21.8
	src4	280×280	1200	Cross	Two $H175 \times 90 \times 5 \times 8$	12 No. 5	100	25.3
Tsai et al. [22]	src5	280×280	1200	Cross	Two $H160 \times 50 \times 3.2 \times 4.5$	4 No. 5	190	26.0
	src6	280×280	1200	Cross	Two $H160 \times 50 \times 3.2 \times 4.5$	4 No. 5	140	26.3
	src7	280×280	1200	Cross	Two $H160 \times 50 \times 3.2 \times 4.5$	12 No. 5	140	25.0
	src8	280×280	1200	Cross	Two $H160 \times 50 \times 3.2 \times 4.5$	4 No. 5	100	26.6
	src9	280×280	1200	Cross	Two $H160 \times 50 \times 3.2 \times 4.5$	12 No. 5	100	24.6
	src10	280×280	1200	Cross	Two $H160 \times 50 \times 3.2 \times 4.5$	12 No. 5	100	24.3
	CL-TE	300×300	1000	T	$H100 \times 50 \times 5 \times 7, H125 \times 60 \times 6 \times 8$	4 No. 6	100	22.9
	CL-TO	300×300	1000	T	$H100 \times 50 \times 5 \times 7, H125 \times 60 \times 6 \times 8$	4 No. 6	100	22.9
Chen et al. [23]	CL-HO	300×300	1000	Cross	$H100 \times 50 \times 5 \times 7, H125 \times 60 \times 6 \times 8$	4 No. 6	100	22.9
	CH-TE	300×300	1000	T	$H150 \times 100 \times 6 \times 9, H175 \times 90 \times 5 \times 8$	4 No. 6	100	31.4
	CH-TO	300×300	1000	T	$H150 \times 100 \times 6 \times 9, H175 \times 90 \times 5 \times 8$	4 No. 6	100	31.4
	CH-HO	300×300	1000	Cross	$H150 \times 100 \times 6 \times 9, H175 \times 90 \times 5 \times 8$	4 No. 6	100	31.4

For the tests by Chen and Yeh, and Tsai et al., three shapes of the structural steel section used in the specimens were I-, H- and cross-shaped sections, as illustrated in Fig. 5. The H-shaped steel section is more like the wide-flange section, while the I-shaped section has a narrow flange. For the tests carried out by Chen et al., a T-shaped steel section was used in the specimens. Fig. 6 depicts the cross section configurations of the composite columns. Table 1 summarizes geometrical properties of the composite stub columns in these three tests.

A total of 26 composite stub columns are included in this study. The main variables are the shape of the structural steel section, longitudinal reinforcing bar and lateral tie. Four types of the structural steel section were used. The regions defined for unconfined, partially and highly confined concrete for various composite cross sections used in these tests are illustrated in Fig. 7. The cross section with cross-shaped steel section results in the largest area of highly confined concrete while I-shaped has the smallest area. Table 2 tabulates all the measured material properties used for analytical prediction.

According to the analytical procedure, the stress–strain curves for unconfined, partially and highly confined concrete are calculated and shown in Fig. 8, which presents the curves for specimens with H- and cross-shaped steel sections. Strength increase for partially confined concrete is primarily due to the lateral reinforcement. However, besides the lateral reinforcement, strength increase for highly confined concrete is further contributed by the confining stress owing to the steel section. As indicated in the figures, the highly confined concrete provides higher strength than partially confined concrete,
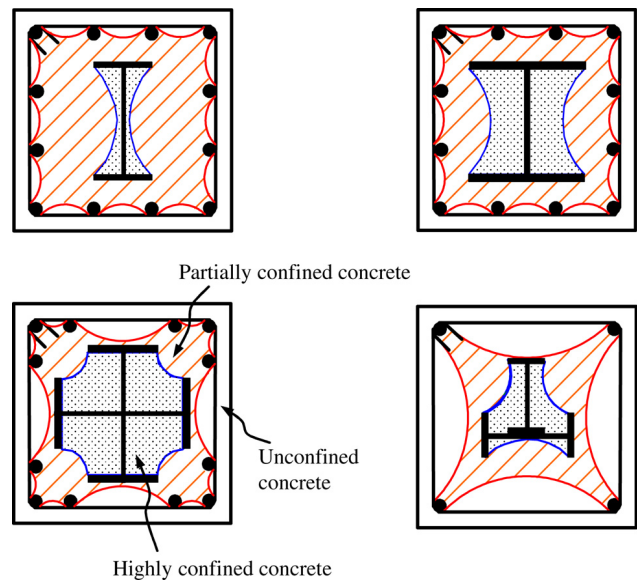

Fig. 7. Regions for unconfined, partially confined, and highly confined concrete in various composite cross sections.

especially for composite cross section with cross-shaped steel section, as shown in Fig. 8(b).

3.2. Comparison of analytical and experimental results

On the basis of strain compatibility and constitutive relationships for material components at a given axial

Table 2
Material properties used for analytical modeling

Specimen	Area of steel A_s (mm^2)	Area of bar A_r (mm^2)	Area of unconfined concrete A_{cu} (mm^2)	Area of partially confined concrete A_{cp} (mm^2)	Area of highly confined concrete A_{ch} (mm^2)	Yield strength of steel f_{ys} (MPa)	Yield strength of bar f_{yr} (MPa)	Concrete strength f'_{co} (MPa)	Confinement factor for partially confined concrete K_p	Confinement factor for highly confined concrete K_h
SRC1	4014	2400	29 955	29 074	12 957	296	350	29.5	1.08	1.23
SRC2	4014	2400	29 955	29 074	12 957	296	350	28.1	1.22	1.24
SRC3	4014	2400	29 955	29 074	12 957	296	350	29.8	1.50	1.50
SRC4	4585	2400	32 086	19 580	19 749	345	350	29.8	1.08	1.87
SRC5	4585	2400	32 086	19 580	19 749	345	350	29.8	1.20	1.90
SRC6	4585	2400	32 086	19 580	19 749	345	350	29.5	1.48	1.97
SRC7	1785	2400	32 086	38 774	3 355	303	350	28.1	1.09	1.10
SRC8	1785	2400	32 086	38 774	3 355	303	350	26.4	1.24	1.24
SRC9	1785	2400	32 086	38 774	3 355	303	350	28.1	1.09	1.10
SRC10	1785	2400	32 086	38 774	3 355	303	350	29.8	1.21	1.21
src1	4585	800	49 753	3 538	19 724	274	453	23.9	1.08	1.86
src2	4585	800	49 753	3 538	19 724	274	453	23.5	1.14	1.88
src3	4585	2400	31 390	20 301	19 724	274	453	21.8	1.25	1.96
src4	4585	2400	31 390	20 301	19 724	274	453	25.3	1.22	1.86
src5	1856	800	49 753	12 657	13 334	271	453	26.0	1.04	1.34
src6	1856	800	49 753	12 657	13 334	271	453	26.3	1.07	1.35
src7	1856	2400	31 390	29 420	13 334	271	453	25.0	1.25	1.37
src8	1856	800	49 753	12 657	13 334	271	453	26.6	1.13	1.35
src9	1856	2400	31 390	29 420	13 334	271	453	24.6	1.22	1.39
src10	1856	2400	31 390	29 420	13 334	271	453	24.3	1.42	1.42
CL-TE	2869	1136	54 674	24 681	6 640	333	388	22.9	1.26	1.26
CL-TO	2869	1136	54 674	24 681	6 640	333	388	22.9	1.26	1.26
CL-HO	2839	1136	54 674	24 521	6 830	333	388	22.9	1.26	1.34
CH-TE	4989	1136	54 674	12 360	16 841	320	388	31.4	1.19	1.31
CH-TO	4989	1136	54 674	12 360	16 841	320	388	31.4	1.19	1.31
CH-HO	4959	1136	54 674	11 943	17 288	320	388	31.4	1.19	1.65

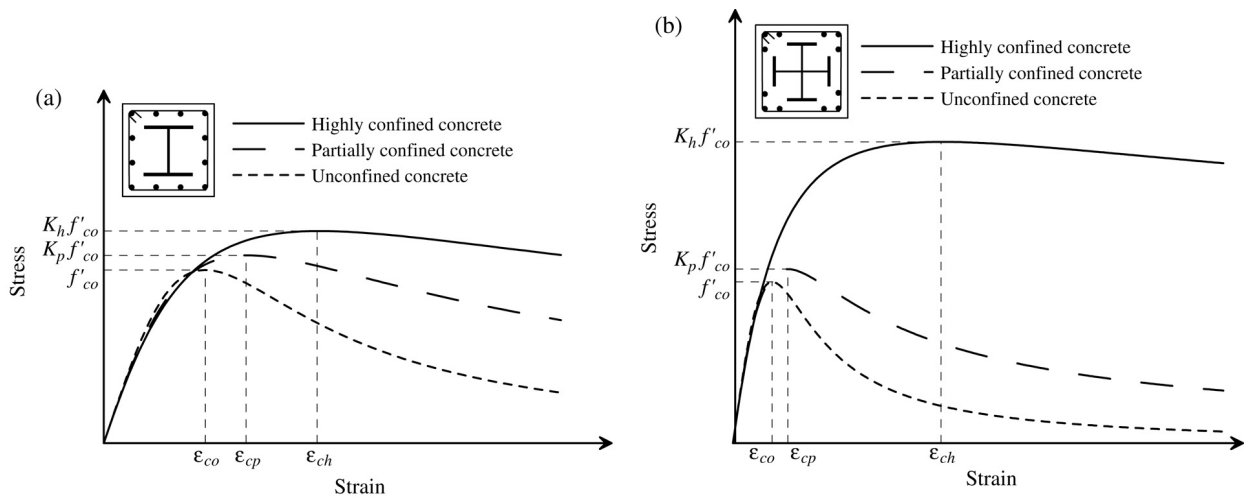Fig. 8. Stress–strain curves for unconfined and confined concrete: (a) H-shaped steel section; (b) cross-shaped steel section.

compressive strain ε, the analytical axial load P_{Analy} is given by

$$P_{\text{Analy}} = f_s A_s + f_{sr} A_r + f_{cu} A_{cu} + f_{cp} A_{cp} + f_{ch} A_{ch} \quad (9)$$

where f_s is the stress of the structural steel; f_{sr} is the stress of the longitudinal bars; f_{cu} is the stress of the unconfined concrete; f_{cp} is the stress of the partially confined concrete; f_{ch} is the stress of the highly confined concrete; A_s is the cross-sectional area of the structural steel section; A_r is the cross-

sectional area of the longitudinal bars; A_{cu} is the area of the unconfined concrete; A_{cp} is the area of the partially confined concrete; and A_{ch} is the area of the highly confined concrete.

The axial load and axial strain relationships for all specimens were calculated by the proposed model. The analytical axial load–strain curves for specimen SRC4 are presented in Fig. 9 in which the curves for each material are included. It is observed that the unconfined concrete reaches its maximum strength at the strain of 0.002. The structural steel and longitudinal bars
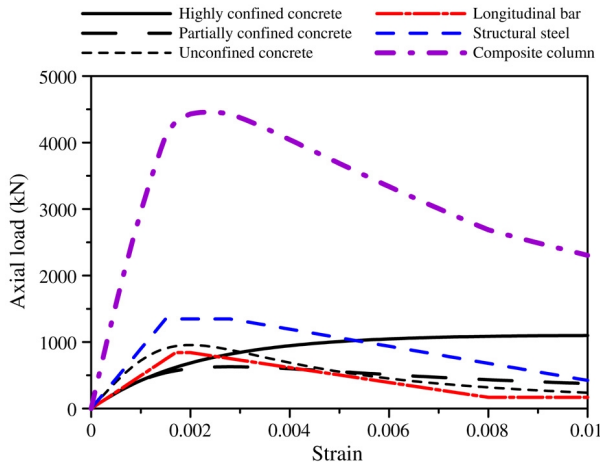
Fig. 9. Analytical axial load–strain curves for specimen SRC4.

have yielded at this strain. After that, the axial resistance of the column still increases due to the strength enhancement from partially and highly confined concrete.

Fig. 10 shows the comparison of analytical and experimental axial load–strain curves for specimens with different structural steel sections. The predicted curves are in good agreement with the experimental results. In addition to the pre-peak behavior, an accurate prediction for the post-peak behavior is obtained. The post-peak behavior results from the use of the degrading model for the longitudinal bars and structural steel as well as the post-peak behavior of the unconfined and partially confined concrete.

Table 3 presents the maximum axial compressive loads of the experimental tests and analytical predictions for all the specimens. The analytical expressions can accurately predict the experimental axial compressive loads. The average ratios of the experimental loads to analytical capacities, P_{Test}/P_{Analy}, are 1.01, 1.02 and 1.00 for three series tests, and the corresponding coefficients of variation are 0.02, 0.06 and 0.02. Among the specimens, the axial capacities of the stub columns are well overestimated in only two columns, src3 and src4, with testing to predicted load ratios of 0.94 and 0.90, respectively. However, the testing axial loads were suspected because of the concrete defect during casting the columns, as reported in the literature [22].

3.3. Squash load of composite stub columns

A squash load calculation is a simplified method to predict the axial compressive capacity for a stub column. Assuming that each material reaches its ultimate strength, the squash load of a composite stub column, P_{Squash}, is defined by:

$$P_{Squash} = 0.85 f'_c A_c + f_{ys} A_s + f_{yr} A_r \tag{10}$$

where f_{ys} is the yield strength of the structural steel; f_{yr} is the yield strength of the longitudinal bar; A_c is the total area of the concrete. It should be noted that $0.85 f'_c$ is used to represent the concrete strength in a structural column. Of course, concrete strength increase owing to the confinement effect is not considered for calculating the squash load. The

concrete confinement is also not taken into account for nominal axial compressive strength in various codes, such as ACI building code [24] and AIJ standards [25].

As presented in Table 3, the squash loads for all stub columns are also compared to the maximum experimental loads. The squash loads were calculated using measured material strengths as presented in Table 2. The average ratios of the experimental loads to squash loads, P_{Test}/P_{Squash}, for three series tests range from 1.11 to 1.15, which are higher than those of P_{Test}/P_{Analy}. The errors of the squash loads compared to the experimental results are generally more than 10% and even up to 21%. The reason for these errors may be attributed to the confinement effect of the concrete. Because of neglect of the concrete confinement, the ratios of P_{Test}/P_{Squash} become large for the columns with large concrete area ratio, as in the case of the columns SRC7~10, src5~10, and CL-series. Nevertheless, the analytical predictions give a fair ratio of P_{Test}/P_{Analy} for columns with different concrete area ratios.

3.4. Confinement factors for partially and highly confined concrete

The strength of the confined concrete is influenced by the tie spacing, volumetric ratio of the lateral reinforcement, and the distribution of the longitudinal reinforcing bar [18]. According to the model for partially confined concrete, the partial confinement factor is highly dependent on the lateral tie spacing for the specimens used in this study. The effect of the tie spacing on the axial load–deformation behavior is shown in Fig. 11, which confirms that reduction of the tie spacing enhances post-peak behavior. Fig. 12 shows the relations of the tie spacing versus confinement factor K_p for partially confined concrete for columns tested by Chen and Yeh. It is apparent that the effectiveness of confinement by the lateral reinforcement is shown in the figure. Small tie spacing results in the increase of the K_p.

The confinement factor K_h for highly confined concrete is influenced by the shape of the structural steel section which provides confining stress on the core concrete. Fig. 13 presents the steel shape versus K_h relations and shows the effect of the steel shape on the effectiveness of confinement. The confining effect is enhanced by the structural steel, particularly by the cross-shaped section. It is because the cross-shaped steel section can provide confining pressure in both directions and result in a higher value of the confinement factor K_h than the I- or H-shaped steel section which confines the concrete in only one direction.

4. Conclusions

An analytical model for determining the axial behavior and capacity of concrete encased composite stub columns is proposed. The following conclusions can be made based on the analytical investigation.

1. Based on strain compatibility, the analytical model can reasonably simulate the axial compressive load–deformation relations of composite stub columns with various steel
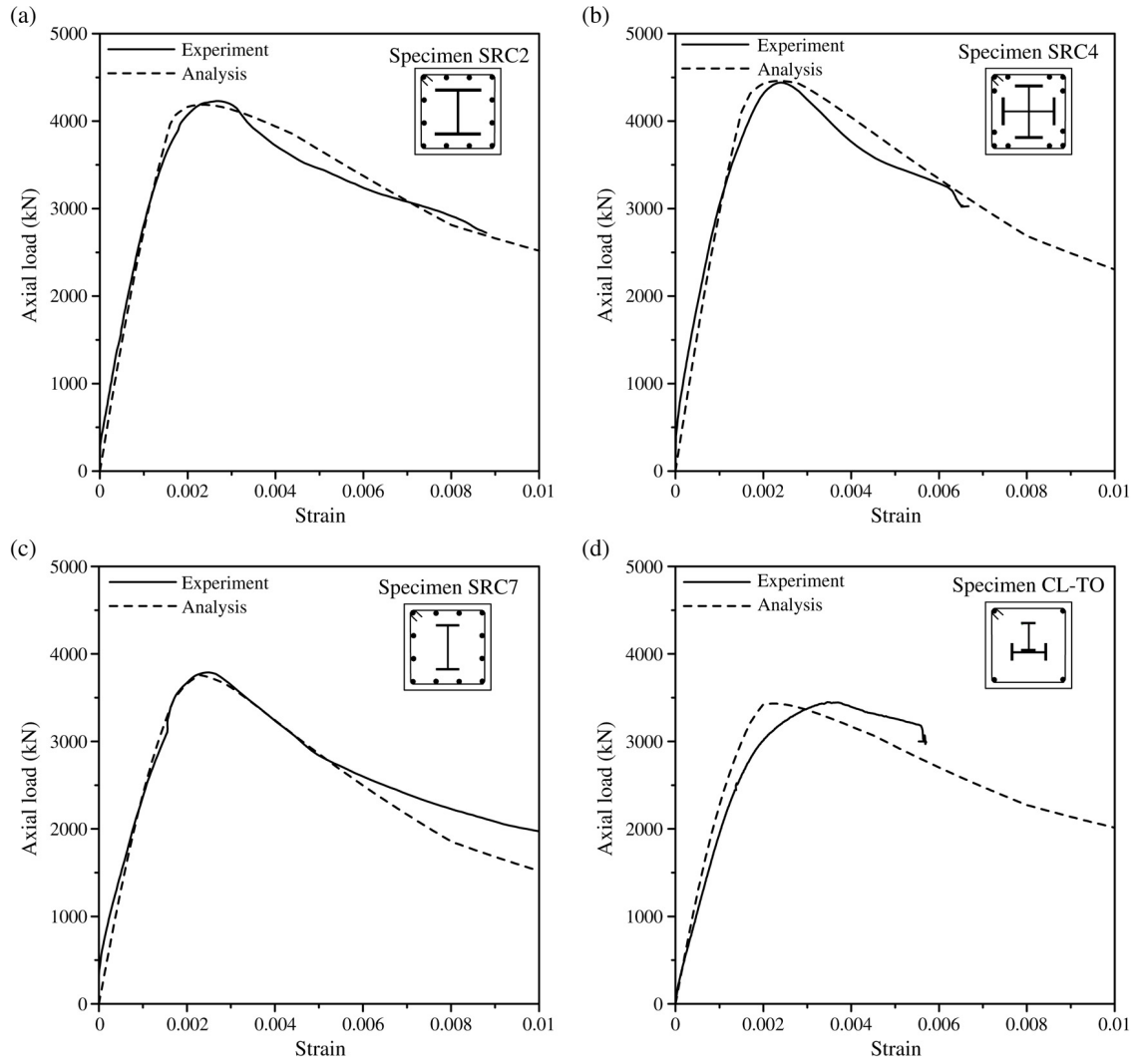
Fig. 10. Comparison of experimental and analytical axial load–strain curves: (a) specimen SRC2; (b) specimen SRC4; (c) specimen SRC7; (d) specimen CL-TO.
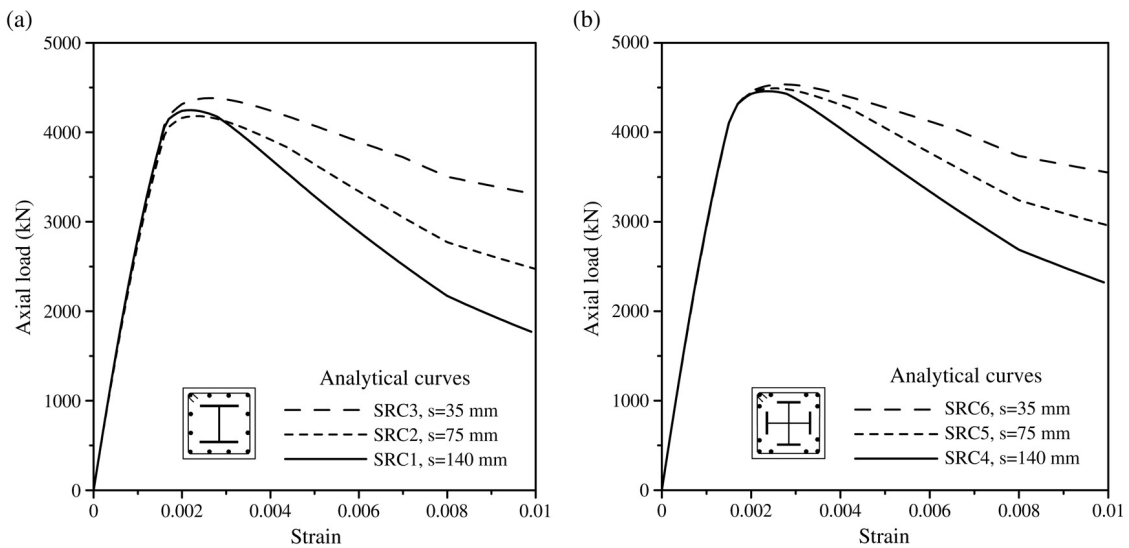

Fig. 11. Effect of tie spacing on axial load–strain curves: (a) H-shaped steel section; (b) cross-shaped steel section.

Table 3
Comparison between experimental and analytical results

| Author	Specimen	Test P_{Test} (kN)	Squash P_{Squash} (kN)	Analysis P_{Analy} (kN)	$\frac{P_{Test}}{P_{Squash}}$	$\frac{P_{Test}}{P_{Analy}}$
	SRC1	4220	3832	4247	1.10	0.99
	SRC2	4228	3748	4180	1.13	1.01
	SRC3	4399	3832	4381	1.15	1.00
	SRC4	4441	4230	4459	1.05	1.00
Chen and Yeh [21]	SRC5	4519	4230	4491	1.07	1.01
	SRC6	4527	4212	4535	1.07	1.00
	SRC7	3788	3154	3758	1.20	1.01
	SRC8	3683	3047	3582	1.21	1.03
	SRC9	3630	3154	3530	1.15	1.03
	SRC10	3893	3260	3693	1.19	1.05
				Average	1.13	1.01
				Coefficient of variation	0.05	0.02
	src1	3602	3101	3486	1.16	1.03
	src2	3502	3076	3462	1.14	1.01
	src3	3836	3666	4062	1.05	0.94
	src4	3854	3818	4304	0.99	0.90
Tsai et al. [22]	src5	3063	2539	2877	1.21	1.06
	src6	3009	2559	2905	1.18	1.04
	src7	3696	3166	3539	1.17	1.04
	src8	3088	2578	2934	1.20	1.05
	src9	3748	3141	3506	1.19	1.07
	src10	3744	3122	3528	1.15	1.06
				Average	1.15	1.02
				Coefficient of variation	0.06	0.06
	CL-TE	3452	3070	3433	1.12	1.01
	CL-TO	3448	3070	3433	1.12	1.00
Chen et al. [23]	CL-HO	3514	3060	3428	1.15	1.03
	CH-TE	4652	4277	4732	1.09	0.98
	CH-TO	4718	4277	4732	1.10	1.00
	CH-HO	4676	4269	4766	1.10	0.98
				Average	1.11	1.00
				Coefficient of variation	0.02	0.02
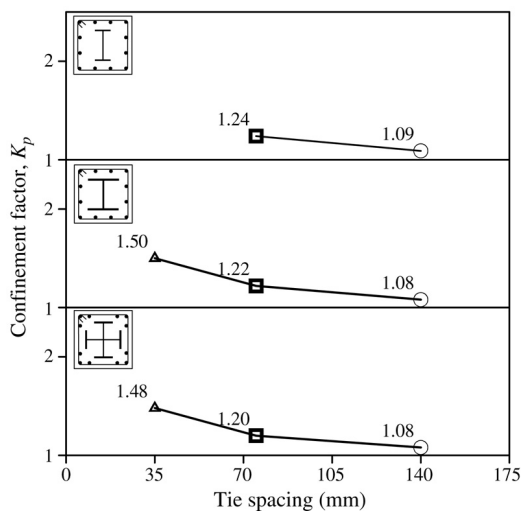
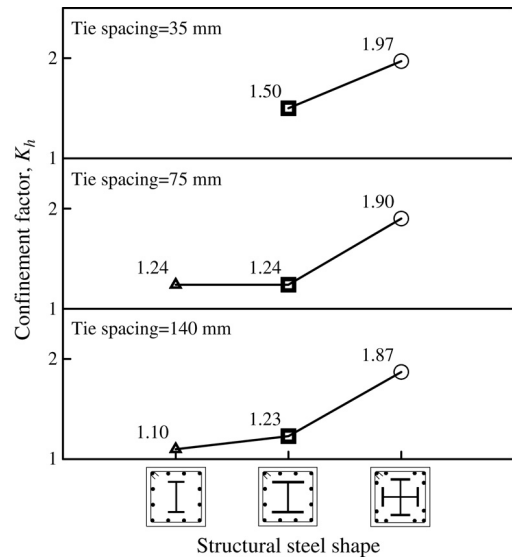Fig. 12. Confinement factor for partially confined concrete.

Fig. 13. Confinement factor for highly confined concrete.

sections, tie spacings, and distributions of the longitudinal bars.

2. The axial compressive loads for 26 composite stub columns can be accurately predicted by the analytical model. The

predictions are better than the squash load. The axial load-carrying capacity of a composite stub column is developed owing to the confinement effect of the concrete.

3. The concrete confinement effect due to the confining stress from the lateral reinforcement as well as different shapes of the structural steel section is established for partially and highly confined concrete. The concrete confinement is confirmed from the comparisons of the predictions with experimental results. The cross-shaped steel section leads to the highest confinement while the I-shaped has the lowest one.

Acknowledgment

References

[1] Roeder CW. Overview of hybrid and composite systems for seismic design in the United States. Engineering Structures 1998;20(4–6): 355–63.

[2] Morino S. Recent developments in hybrid structures in Japan — research, design and construction. Engineering Structures 1998;20(4–6):336–46.

[3] Brettle HJ. Ultimate strength design of composite columns. Journal of the Structural Division, ASCE 1973;99(9):1931–51.

[4] Bridge RQ, Roderick JW. Behavior of built-up composite columns. Journal of the Structural Division, ASCE 1978;104(7):1141–55.

[5] Furlong RW. Concrete encased steel columns — design tables. Journal of the Structural Division, ASCE 1974;100(9):1865–82.

[6] Mirza SA, Skrabek BW. Statistical analysis of slender composite beam–column strength. Journal of Structural Engineering 1992;118(5): 1312–32.

[7] El-Tawil S, Deierlein GG. Strength and ductility of concrete encased composite columns. Journal of Structural Engineering 1999;125(9): 1009–19.

[8] Mirza SA, Hyttinen V, Hyttinen E. Physical tests and analyses of composite steel–concrete beam–columns. Journal of Structural Engineering 1996;122(11):1317–26.

[9] Li L, Sakai J, Matsui C. Seismic behavior of steel encased reinforced concrete beam–columns. In: Proceedings of the international conference on advances in structures. 2003. p. 1201–7.

[10] Ricles JM, Paboojian SD. Seismic performance of steel-encased composite columns. Journal of Structural Engineering 1994;120(8): 2474–94.

[11] Susantha KAS, Ge H, Usami T. Uniaxial stress–strain relationship of concrete confined by various shaped steel tubes. Engineering Structures 2001;23(10):1331–47.

[12] Han LH. Tests on stub columns of concrete-filled RHS sections. Journal of Constructional Steel Research 2002;58:353–72.

[13] O'Shea MD, Bridge RQ. Design of circular thin-walled concrete filled steel tubes. Journal of Structural Engineering 2000;126(11):1295–303.

[14] Sakino K, Nakahara H, Morino S, Nishiyama I. Behavior of centrally loaded concrete-filled steel-tube short columns. Journal of Structural Engineering 2004;130(2):180–8.

[15] Giakoumelis G, Lam D. Axial capacity of circular concrete-filled tube columns. Journal of Constructional Steel Research 2004;60:1049–68.

[16] Schneider SP. Axially loaded concrete-filled steel tubes. Journal of Structural Engineering 1998;124(10):1125–38.

[17] Sheikh SA, Uzumeri SM. Analytical model for concrete confinement in tied columns. Journal of the Structural Division, ASCE 1982;108(12): 2703–22.

[18] Mander JB, Priestley MJN, Park R. Theoretical stress–strain model for confined concrete. Journal of Structural Engineering 1988;114(8): 1804–26.

[19] Kent DC, Park R. Flexural members with confined concrete. Journal of the Structural Division, ASCE 1971;97(7):1969–90.

[20] Bayrak O, Sheikh SA. Plastic hinge analysis. Journal of Structural Engineering 2001;127(9):1092–100.

[21] Chen CC, Yeh SC. Ultimate strength of concrete encased steel composite columns. In: Proceedings of the third national conference on structural engineering. 1996. p. 2197–206 [in Chinese].

[22] Tsai KC, Lien Y, Chen CC. Behavior of axially loaded steel reinforced concrete columns. Journal of the Chinese Institute of Civil and Hydraulic Engineering 1996;8(4):535–45 [in Chinese].

[23] Chen CC, Weng CC, Lin IM, Li JM. Seismic behavior and strength of concrete encased steel stub columns and beam–columns. Report no. MOIS 881012-1. Architecture and Building Research Institute; 1999 [in Chinese].

[24] American Concrete Institute. Building code requirements for structural concrete (ACI 318-02) and Commentary (ACI 318R-02). Detroit; 2002.

[25] Architectural Institute of Japan. AIJ standards for structural calculation of steel reinforced concrete structures. 1991.